

A revisit to scalar dark matter with radiative corrections

Shankha Banerjee¹ and Nabarun Chakrabarty²

¹*LAPTH, Univ. de Savoie, CNRS, B.P.110, F-74941 Annecy-le-Vieux, France*

²*Regional Centre for Accelerator-based Particle Physics,
Harish-Chandra Research Institute, HBNI,
Chhatnag Road, Jhusi, Allahabad 211019, India*

Abstract

Extended Higgs sectors have been studied extensively in context of dark matter phenomenology in tandem with other aspects. In this study, we compute radiative corrections to the dark matter-Higgs portal coupling, which is in fact a common feature of all scalar dark matter models irrespective of the hypercharge of the multiplet from which the dark matter candidate emerges. We select the popular Inert Doublet Model (IDM) as a prototype in order to demonstrate the impact of the next-to-leading order corrections, thereby probing the plausibility of extending the allowed parameter space through quantum effects. This turns out to be true since the loop corrections are sizeable in magnitude even in a scenario where all the inert scalars are decoupled. Given that the tree level portal coupling is a *prima facie* free parameter, the percentage change from loop effects can be large. This modifies the dark matter phenomenology at a quantitative level. It also encourages one to include loop corrections to all other interactions that are deemed relevant in this context.

I. INTRODUCTION.

The successful discovery of the Higgs boson in 2012 by the CMS [1] and ATLAS [2] collaborations completed the search for the last missing piece in the Standard Model (SM) of particle physics. However, SM is unable to answer certain fundamental observations, *viz.*, the existence of dark matter (DM), massive neutrinos, the excess of baryons over anti-baryons, three generations of leptons etc. Besides, there are certain theoretical issues like the hierarchy problem, which the SM fails to answer. We are thus led to consider physics beyond the standard model (BSM) in order to explain such observations. After the discovery of the Higgs boson, the theoretical and experimental community have spent all their resources in studying the couplings and the CP nature of this discovered boson. Except for a few deviations like the $t\bar{t}h$ signal strength [3, 4], the coupling strengths of the Higgs boson to other SM particles conform with their SM expectations within 2σ uncertainties. A purely CP odd scenario is also shown to be disfavoured by experiments. The invisible branching ratio of an SM-like Higgs boson is also constrained by experiments and global fits to $\lesssim 20\%$ at 95% CL. The high-luminosity run of the LHC (HL-LHC) has the potential to constrain all the Higgs couplings to an even greater precision. Besides, it also promises to shed light on the cubic and quartic couplings of the Higgs boson through its pair production.

On the other hand, the existence of dark matter in the universe has been repeatedly verified by astrophysical and cosmological observations ranging from galactic to cosmological scales. Apart from the fact that dark matter interacts gravitationally, the only quantitative aspect that we know about it is its relic abundance [5], $\Omega_c h^2 = 0.1199 \pm 0.0027$. However, its nature is still unknown and we expect it to be some electrically neutral particle with no colour quantum number. Amidst the various propositions, the Weakly Interacting Massive Particle (WIMP) stands out as one of the most attractive candidates by attributing to its simplicity and predictability. The observed relic abundance can be explained by the thermal freeze-out mechanism of the WIMP, when its mass is around the electroweak scale. An extension of the SM with a WIMP can help us understand better the origin of the electroweak symmetry breaking (EWSB). The predicted interactions of the WIMP with the SM particles greatly motivate the experimental community to search for this elusive particle at collider experiments, direct dark matter detection experiments at underground laboratories and from indirect detections from cosmological and astrophysical observations.

The lightest supersymmetric particle (LSP) has been considered as the most attractive candidate for cold dark matter due to the fact that the supersymmetric (SUSY) theories alleviate most of the aforementioned limitations faced by the SM. Unfortunately however, SUSY models are gradually getting severely constrained because of the lack of any evidence for superpartners. Lack of any conclusive signatures of WIMPs have gradually pushed the celebrated WIMP scenarios to the corner. In the present study we take recourse to one of the simplest models, the inert Higgs doublet model (IDM) [6] which has an inbuilt WIMP candidate. The IDM is possibly the simplest limit of a general two Higgs doublet model, where the additional doublet consisting of complex scalar fields only couples to the SM Higgs and gauge bosons and not to the fermions. However, the most interesting aspect of this model is that the additional doublet is odd under a \mathbb{Z}_2 symmetry

rendering the occurrence of an even number of *inert* particles at any interaction vertex. It has also been shown that the neutral scalar or pseudoscalar in the additional doublet can be considered as WIMPs and hence as a viable cold dark matter candidate in the universe [7, 8]. In this model, obtaining the correct relic abundance does not require a fine tuning but only requires adjusting its couplings or through co-annihilation with another particle [9]. Several experiments like LUX [10], SuperCDMS [11], Fermi-LAT [12, 13] and AMS-02 [14, 15] have tested the dark matter scenario in the context of WIMP searches. These direct dark matter searches have now constrained the mass of the dark matter candidate in the IDM to around half of the mass of the SM Higgs boson (125 GeV) or above ~ 500 GeV [16–18]. The resonance mass around ~ 62 GeV might still not be completely excluded in the future [19] by direct detection experiments like XENON1T [20] and LZ [21]. Outside these ranges, the dark matter candidate can only contribute to a fraction of the total thermal relic density. Because of its simplicity and richness, the IDM has been exhaustively studied in astrophysical and cosmological studies [22–27] and studies pertaining to collider physics [28–35]. There have been several studies in the context of the LHC which considers the Drell-Yan production of HA or H^+H^- [36–38] and then further decays of $H \rightarrow AZ^{(*)}$, $H^\pm \rightarrow AW^{\pm(*)}$ to yield a final state of dileptons or dijets + \cancel{E}_T . Here H and A are the additional neutral scalar and pseudoscalar respectively and H^\pm is the charged scalar in this doublet. Depending on the HHh coupling, a monojet signature can also be looked for at the LHC by a pair production of these scalars, if H is the dark matter candidate. To give a broad picture, IDM connects the Higgs to dark matter by acting as a portal between the visible and the invisible sector. The on-shell corrections to hVV , hff and hhh couplings have recently been obtained in Refs. [39, 40] after considering constraints from perturbative unitarity, vacuum stability and relic abundance. The corrections have been shown to be substantial and can be $\simeq 100\%$ in the regime of light dark matter masses. These calculations will be of immense importance when the experiments start to bound the cubic and quartic higgs self-couplings. It has been shown in Ref. [41] that the electroweak corrections to the direct detection cross-sections in the IDM can be substantial.

In the present work, we revisit the electroweak correction of the HHh vertex and show its effects on the relic abundance calculation and the direct detection cross-section. We are guided by the principle that in order to ascertain the importance of any model for dark matter searches, one needs to look at the higher order corrections which will lead to a significant shift in the parameter space under the constraints from relic density, direct detection cross-section, oblique corrections and collider limits. IDM is one of the simplest models to test our claim and through this we show the importance of precision measurements in the dark matter sector.

We organise the paper as follows: In section II, we briefly sketch the model and its important aspects. We outline the constraints coming from perturbativity, vacuum stability etc. in section III. We discuss our renormalisation procedure in section IV but leave all the details in Appendix VII. In section V, we discuss the numerical results and finally we summarise and conclude in section VI.

II. MODEL DETAILS.

In addition to the SM fields, the inert doublet model employs an additional scalar doublet (Φ_2). Moreover, the framework is endowed with a global \mathbb{Z}_2 symmetry under which Φ_2 has negative charge whereas the SM fields have positive charge. The most general renormalisable scalar potential involving two doublets is then given by [40]

$$V = \mu_1^2 \Phi_1^\dagger \Phi_1 + \mu_2^2 \Phi_2^\dagger \Phi_2 + \frac{\lambda_1}{2} (\Phi_1^\dagger \Phi_1)^2 + \frac{\lambda_2}{2} (\Phi_2^\dagger \Phi_2)^2 + \lambda_3 (\Phi_1^\dagger \Phi_1) (\Phi_2^\dagger \Phi_2) + \lambda_4 (\Phi_2^\dagger \Phi_1) (\Phi_1^\dagger \Phi_2) + \left[\frac{\lambda_5}{2} (\Phi_1^\dagger \Phi_2)^2 + \text{h.c.} \right] \quad (1)$$

where all parameters are real, and Φ_1 is the SM Higgs doublet.

Noting that the \mathbb{Z}_2 symmetry prevents Φ_2 from picking a vacuum expectation value (VEV), enables us to parametrise the doublets directly in terms of the physical scalars as

$$\Phi_1 = \begin{pmatrix} G^+ \\ \frac{1}{\sqrt{2}}(v + h + iG) \end{pmatrix} \quad \text{and} \quad \Phi_2 = \begin{pmatrix} H^+ \\ \frac{1}{\sqrt{2}}(H + iA) \end{pmatrix} \quad (2)$$

The masses are found to be

$$\begin{aligned} m_h^2 &= \lambda_1 v^2 \\ m_{H^\pm}^2 &= \mu_2^2 + \frac{1}{2} \lambda_3 v^2 \\ m_H^2 &= \mu_2^2 + \frac{1}{2} \lambda_L v^2 \\ m_A^2 &= \mu_2^2 + \frac{1}{2} \lambda_A v^2 \end{aligned} \quad (3)$$

where $\lambda_{L/A} = (\lambda_3 + \lambda_4 \pm \lambda_5)$. The value of λ_1 is determined using $m_h = 125$ GeV.

We choose h to be the SM Higgs with mass ~ 125 GeV. It is easily seen that H, A, H^\pm are rendered stable by the \mathbb{Z}_2 symmetry. Consequently, H and A are potential candidates for DM. While a detailed account of DM phenomenology of the IDM can be found in [28–35], a few statements are still in order. Relic abundance in the PLANCK ballpark is achieved in the two mass regions (a) $50 \lesssim m_{DM} \lesssim 80$ and (b) $m_{DM} \gtrsim 500$ GeV. In region (a), annihilation dominantly proceeds through the exchange of an s -channel h . The sub-dominant contribution to the relic density comes from the t -channel processes to vector boson final states mediated by A and H^\pm . On the other hand, one must have $m_H \simeq m_A \simeq m_{H^\pm}$ in order to generate $\Omega_{DM} h^2 \simeq 0.1$ in region (b). Co-annihilation thus becomes inevitable in this case.

In this study, H is chosen to be the DM candidate. A crucial observation that emerges is, in region (a), $\Omega_{DM} h^2 \simeq$ is highly sensitive to the value of the HHh trilinear coupling ($= -\lambda_L v$). This motivates one to review the entire phenomenology by incorporating radiative corrections to, if not all parameters, to this important interaction nonetheless. It is expected that the impact of a loop-corrected λ_L on relic will be more pronounced in region (a) compared to region (b). In addition, beyond the leading order, the parameters that do not participate in the tree level phenomenology of region (a) (such as λ_2 and masses of the CP-odd and charged scalars), will now have their respective roles in the ensuing quantum effects.

III. CONSTRAINTS.

Our goal is to take a recourse to the DM phenomenology in the IDM after carrying out one-loop corrections to the HHh coupling. In the process, we obey various constraints stemming from both theory and experiments. On the theoretical side, perturbativity, unitarity and vacuum stability can appreciably constrain an extended Higgs sector as in the IDM. $|\lambda_i| \leq 4\pi$ ($i=1,5$). The $2 \rightarrow 2$ amplitude matrix corresponding to scattering of the longitudinal components of the gauge bosons can be mapped to a corresponding matrix for the scattering of the goldstone bosons [42–45]. The theory respects unitarity if the absolute value of each eigenvalue of the aforementioned amplitude matrix does not exceed 8π .

The tree-level potential remains positive definite along various directions in field space if the following conditions are met [40],

$$\lambda_1(Q) > 0 \tag{4a}$$

$$\lambda_2(Q) > 0 \tag{4b}$$

$$\lambda_3(Q) + \sqrt{\lambda_1(Q)\lambda_2(Q)} > 0 \tag{4c}$$

$$\lambda_3(Q) + \lambda_4(Q) - |\lambda_5(Q)| + \sqrt{\lambda_1(Q)\lambda_2(Q)} > 0 \tag{4d}$$

On the experimental side, the bounds on the oblique parameters are taken into account. The most prominent of these is the constraint on the T parameter which puts restriction on the splitting between the \mathbb{Z}_2 odd scalars. We use the NNLO global electroweak fit results obtained by the Gfitter group [46],

$$\Delta S = 0.05 \pm 0.11, \Delta T = 0.09 \pm 0.13 \tag{5}$$

In the absence of any mixing between h and the \mathbb{Z}_2 odd scalars, the tree level couplings of h with fermions and gauge bosons remain unaltered with respect to their SM values. However, the IDM still confronts data on Higgs signal strengths through a modified $h\gamma\gamma$ effective coupling, which now carries the effect of H^+ in the loop. In other words, ensuring $\mu_{\gamma\gamma}$ to lie within the experimental uncertainties, implies that the analysis respects the latest combined signal strength at $7 + 8$ TeV from ATLAS and CMS [47], *viz.*,

$$\mu_{\gamma\gamma} = 1.14^{+0.19}_{-0.18}. \tag{6}$$

Lastly, the LEP exclusion limits have been imposed as $m_A > 100$ GeV and $m_{H^+} > 90$ GeV.

IV. OUTLINE OF RENORMALISATION.

In this section, we present an outline of the renormalisation procedure adopted in [40]. The absence of mixing between h and the inert scalars simplifies the machinery to some extent. The IDM scalar sector can be conveniently described using $\{m_h, v, \mu_2, m_H, m_A, m_{H^+}, \lambda_2, T_h\}$ as independent parameters. Here T_h denotes the tadpole parameter for h . The necessary counter-terms are generated by shifting these parameters

about their renormalised values.

$$m_h^2 \rightarrow m_h^2 + \delta m_h^2 \quad (7a)$$

$$v \rightarrow v + \delta v \quad (7b)$$

$$\mu_2^2 \rightarrow \mu_2^2 + \delta \mu_2^2 \quad (7c)$$

$$m_H^2 \rightarrow m_H^2 + \delta m_H^2 \quad (7d)$$

$$m_A^2 \rightarrow m_A^2 + \delta m_A^2 \quad (7e)$$

$$m_{H^+}^2 \rightarrow m_{H^+}^2 + \delta m_{H^+}^2 \quad (7f)$$

$$\lambda_2 \rightarrow \lambda_2 + \delta \lambda_2 \quad (7g)$$

Note that we do not need to compute the shift in T_h in our case. Moreover, wave-function renormalisation is invoked as

$$\phi \rightarrow (1 + \frac{1}{2} \delta Z_\phi) \phi \quad (8)$$

where $\phi = h, H, A, H^+$.

A more detailed treatment of the renormalisation scheme can be found in [40, 48]. We list here the final results only for brevity.

$$\delta m_\phi^2 = \Pi_{\phi\phi}(m_\phi^2) \quad (9a)$$

$$\delta Z_\phi = -\frac{d}{dp^2} \Pi_{\phi\phi}(p^2)|_{p^2=m_\phi^2} \quad (9b)$$

The quantity of central importance in this study is the renormalised HHh form factor which replaces its tree level counterpart in dark matter calculations. We denote it by $\Gamma_{HHh}^{\text{ren}}$ and decompose it as

$$\Gamma_{HHh}^{\text{ren}}(p_1^2, p_2^2, p^2) = \Gamma_{HHh}^{\text{tree}} + \Gamma_{HHh}^{\text{1PI}}(p_1^2, p_2^2, p^2) + \delta \Gamma_{HHh} \quad (10)$$

Here, p_1, p_2 and $p = p_1 + p_2$ refer respectively to the momenta of the two annihilating H and h respectively. In the right hand side, the first term refers to the tree level form factor. The second and the third respectively denote the unrenormalised 1PI amplitude at the one-loop level; and the corresponding counter-term. It is necessary to express the tree level form factor in terms of the independent parameters in order to generate the corresponding counter-term.

$$\Gamma_{HHh}^{\text{tree}} = -\frac{2}{v}(m_H^2 - \mu_2^2) \quad (11)$$

Leading to

$$\delta \Gamma_{HHh} = -\frac{2(m_H^2 - \mu_2^2)}{v} \left[\frac{\delta m_H^2 - \delta \mu_2^2}{m_H^2 - \mu_2^2} - \frac{\delta v}{v} + \frac{1}{2} \delta Z_h + \delta Z_H \right] \quad (12)$$

Now, we have fixed the counterterms δm_H^2 , δZ_h and δZ_H from Eq. 9. We also know the expression of δv from SM. The only ambiguity in order to fix $\delta \Gamma_{HHh}$ is $\delta \mu_2^2$. There can be several ways to fix this

counter-term. What we choose in the present paper is demand that a physical quantity, here the decay width $h \rightarrow HH$ does not deviate *w.r.t* its tree level value upon including one-loop corrections. This implies¹

$$\delta\Gamma_{HHh} = -\Gamma_{HHh}^{1\text{PI}}(m_H^2, m_H^2, m_h^2) \quad (13)$$

and

$$\delta\mu_2^2 = -\left[\left(\frac{\Gamma_{HHh}^{1\text{PI}}(m_H^2, m_H^2, m_h^2)v}{2(m_H^2 - \mu_2^2)} + \frac{\delta v}{v} - \frac{1}{2}\delta Z_h - \delta Z_H\right)(m_H^2 - \mu_2^2) - \delta m_H^2\right]. \quad (14)$$

Upon considering all these counter-terms, we get an effective correction of the form

$$\Gamma_{HHh}^{\text{ren}}(p_1^2, p_2^2, p^2) = \Gamma_{HHh}^{\text{tree}} + \Gamma_{HHh}^{1\text{PI}}(p_1^2, p_2^2, p^2) - \Gamma_{HHh}^{1\text{PI}}(m_H^2, m_H^2, m_h^2) \quad (15)$$

The counter-terms for the independent parameters are thus fixed. The quantity directly entering into our analysis is $\Gamma_{HHh}^{\text{ren}}(p_1^2, p_2^2, p^2)$. The expressions for the various two- and three-point 1PI amplitudes are relegated to the appendix VII.

V. NUMERICAL RESULTS.

The quantity directly entering into our analysis is $\Gamma_{HHh}^{\text{ren}}(p_1^2, p_2^2, p^2)$. Since dark matter particles annihilate manifestly in an on-shell fashion, we take $p_1^2 = p_2^2 = m_H^2$. Further, cold dark matter particles are non-relativistic, and this allows us to write $p^2 = 4m_H^2$.² This allows us to treat $\lambda_L + \Gamma_{HHh}^{\text{ren}}(m_H^2, m_H^2, 4m_H^2)$ as an "effective" coupling in the present analysis.

Following are the values chosen for the SM parameters:

$m_h = 125.0$ GeV, $m_t = 173.2$ GeV, $m_b = 4.7$ GeV, $m_W = 80.3$ GeV, $m_Z = 91.2$ GeV. The model points are sampled randomly through a scan of the parameter space within the specified ranges,

$$\begin{aligned} \mu_2^2 &\in [0 \text{ GeV}^2, 10^6 \text{ GeV}^2] \\ m_A &\in [100 \text{ GeV}, 500 \text{ GeV}] \\ m_{H^\pm} &\in [100 \text{ GeV}, 500 \text{ GeV}] \end{aligned}$$

We avoid choosing $\mu_2^2 < 0$ in order to prevent the inert doublet picking up a VEV, alongside obeying the vacuum stability, perturbativity and unitarity constraints described in section III. Since, the DM self-interaction λ_2 cannot be directly constrained, we choose $\lambda_2 = 2.0$ in our scans. We remind that the upper bound on the invisible branching fraction of h remains an important constraint whenever $m_H < m_h/2$. Therefore, we require $\text{BR}(h \rightarrow \text{inv}) < 0.15$ which leads to $|\lambda_L + \Gamma_{HHh}^{\text{ren}}| < 0.05$ for $m_H = 55$ GeV for

¹ We assume that this holds even when the decay $h \rightarrow HH$ is kinematically forbidden. The three point C functions are in calculable when $m_H^2 > m_h^2/2$. So in Eqs. 13,14 and 15, we set $m_H^2 = m_h^2/2$.

² We must note that even taking a p^2 off-resonance will yield the same result because the vertex correction will be a function $f(p^2 - m_h^2)$ which will partially cancel with the propagator $\sim \frac{1}{p^2 - m_h^2}$ and the correction will be a "constant" one.

instance, and a tighter bound for lower masses. We focus on the regions $50.0 \text{ GeV} < m_H < 80.0 \text{ GeV}$ and $m_H > 500.0 \text{ GeV}$ (see section II) to illustrate the results.

A. $50.0 \text{ GeV} < m_H < 80.0 \text{ GeV}$

We adopt the more conservative perturbative bound $|\lambda_i| < 2$ and propose the following benchmarks accordingly.

Benchmark	m_A	m_{H+}	λ_L
BP1a	100 GeV	110 GeV	0.001
BP1b	200 GeV	210 GeV	0.001
BP2a	100 GeV	110 GeV	-0.001
BP2b	200 GeV	210 GeV	-0.001
BP3a	100 GeV	110 GeV	0.01
BP3b	200 GeV	210 GeV	0.01
BP4a	100 GeV	110 GeV	-0.01
BP4b	200 GeV	210 GeV	-0.01
BP5a	100 GeV	110 GeV	0.1
BP5b	200 GeV	210 GeV	0.1
BP6a	100 GeV	110 GeV	-0.1
BP6b	200 GeV	210 GeV	-0.1

TABLE I: Benchmark points chosen to illustrate the effect of the one-loop corrections.

The benchmarks are illustrative in nature and they do not exhaust the entire parameter space. The inert scalars in the loops mostly generate a positive contribution to λ_L for $m_H < m_W$. Sometimes a negative correction is also noted due to some one-loop graphs yielding large enough negative contributions by virtue of negative quartic prefactors. Note that these results reflect upon the *non-decoupling* feature of the $m_H < 80 \text{ GeV}$ region, where all component scalars of the extra doublet cannot be simultaneously heavy. As m_A and m_{H+} are increased, the loop correction gets suppressed. This is revealed upon an inspection of Fig. 1, where BP1a exhibits a larger radiative correction compared to BP1b. In fact, the loop enhancement to the portal interaction is as large as $\sim 60 \%$ in case of BP1a. This does not come as a surprise since the tree level magnitude is less in BP1a and BP1b, and the loop effects themselves contribute in the $O(0.0001)$ ballpark, further causing the loop corrected Ωh^2 to drop with respect to the tree level value.

BP2a, BP2b, BP3a, BP3b (see Fig. 1 and Fig. 2) reflect the same qualitative pattern. In some benchmarks however (BP2a and BP4a for example), the absolute value of the effective portal strength diminishes owing to a positive $\Gamma_{HHh}^{\text{ren}}(m_H^2, m_H^2, 4m_H^2)$ adding up to a negative λ_L . More precisely, one finds $\Gamma_{HHh}^{\text{ren}}(m_H^2, m_H^2, 4m_H^2) < |\lambda_L|$ in these cases, such that, the effective coupling is negative and $< |\lambda_L|$. Con-

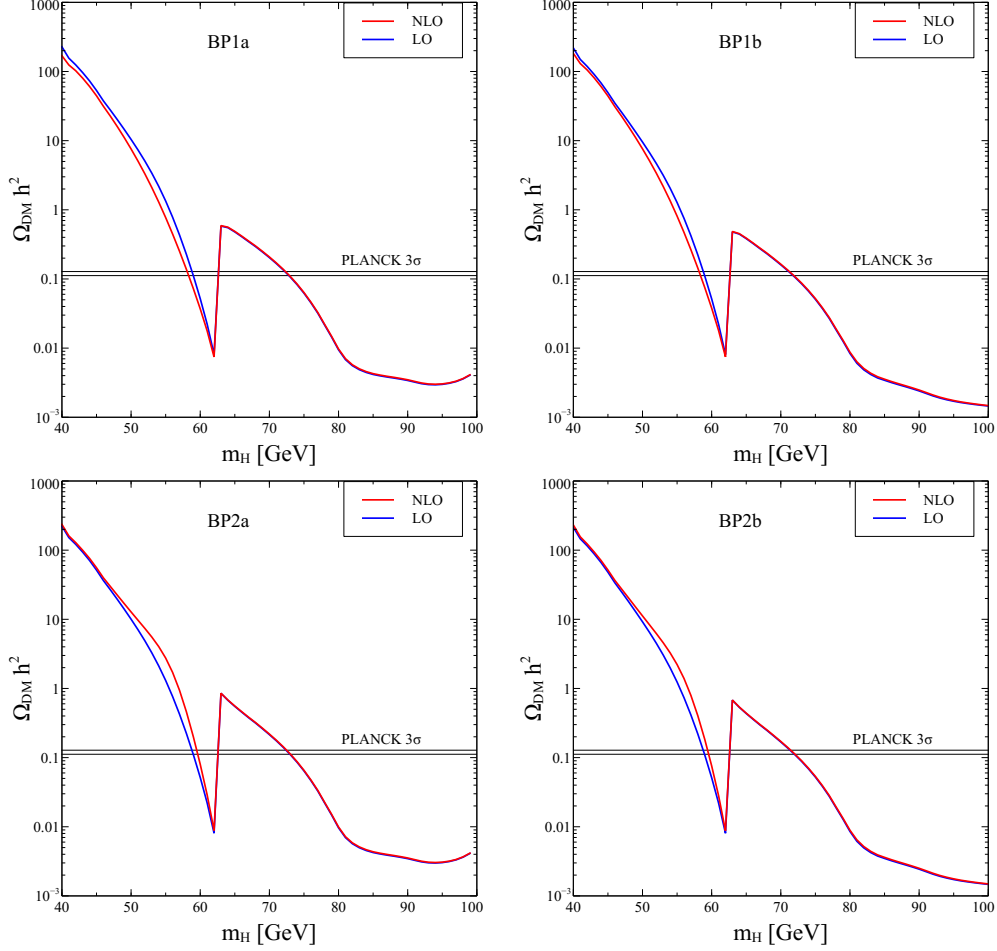


FIG. 1: Variation of the thermal relic with the DM mass. The tree level and one-loop values are denoted by the blue and red curves respectively.

sequently, Ωh^2 is higher than its corresponding tree level value for $m_H < \frac{m_h}{2}$ GeV.

More benchmarks with $\lambda_L < 0$ can witness a loop-driven increment in the relic density in a manner outlined above, if the inert scalar masses are in the appropriate ball-park. For instance, BP6a and BP6b in Fig. 3 highlight this very feature as do BP4a and BP4b. In all, when loop effects are considered, the sign of λ_L can become important in deciding the magnitude of Ωh^2 , unlike tree level annihilations.

Fig. 4 shows the change in the spin-independent dark matter-nucleon scattering rate under radiative corrections. The rate being proportional to $|\lambda_L + \Gamma_{HHh}^{\text{ren}}(m_H^2, m_H^2, 4m_H^2)|^2$, increases upon increasing the effective portal coupling through loop effects and vice versa. We plot the direct detection rates for BP3a and BP6b in Fig. 4 to demonstrate this effect.

The sharp dip in σ_{SI}^p for BP3a occurs because of a cancellation between a positive λ_L and a negative $\Gamma_{HHh}^{\text{ren}}(m_H^2, m_H^2, 4m_H^2)$ observed when $m_H > \frac{m_h}{2}$.

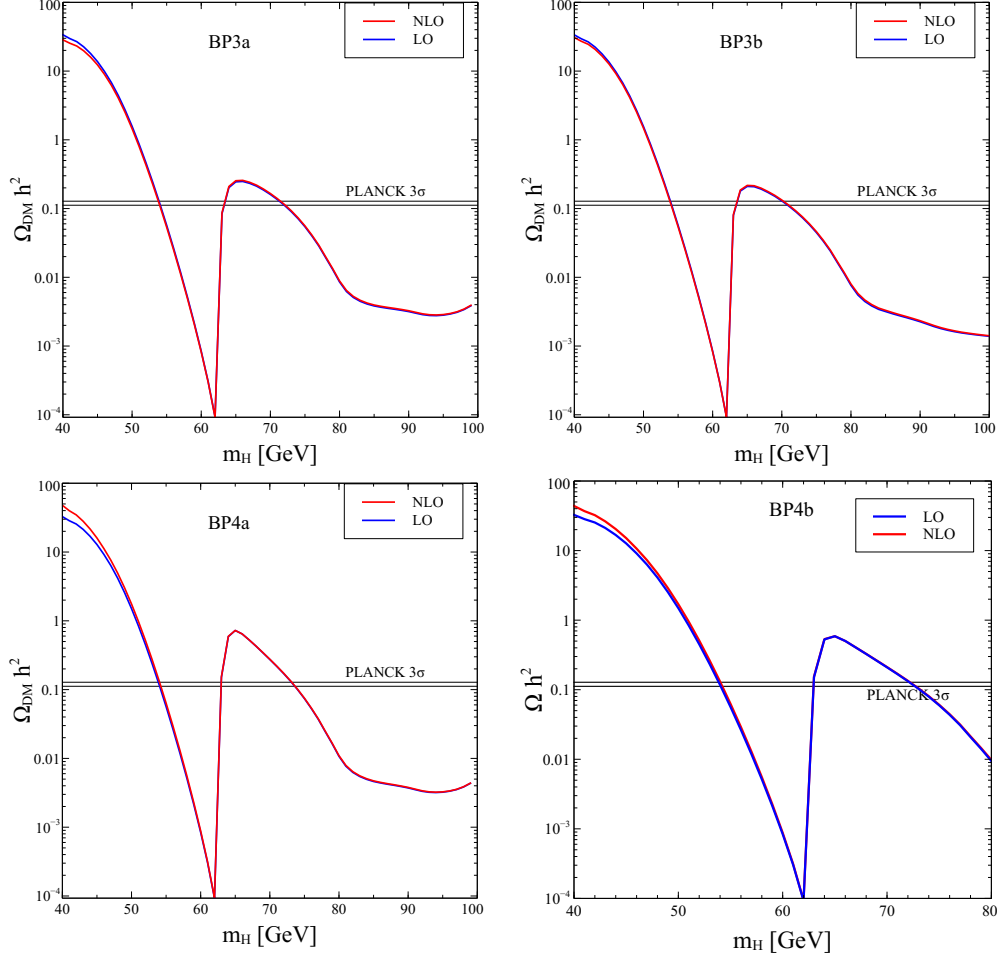


FIG. 2: Variation of the thermal relic with the DM mass. The tree level and one-loop values are denoted by the blue and red curves respectively.

B. $m_H > 500.0$ GeV

For this part, we choose $m_A = m_H + 2$ GeV and $m_{H^+} = m_H + 4$ GeV to trigger the requisite co-annihilations, along with setting $\lambda_L = 0.01$. The radiative correction to λ_L is found to be negative for this part (see Fig. 5). It is approximately $\simeq -40\%$ when the masses nearly equal 1 TeV. The effective portal strength thus diminishes. It thereby raises the thermal relic only slightly with respect to its tree level value. This is because the relic mostly comes from co-annihilations and not through h mediated annihilations in this region. However, a cancellation between the tree level and one-loop form factors is expected for a higher value of λ_L , that could raise Ωh^2 to the PLANCK 3σ band.

It is seen that the deviations in relic density and direct detection rates *w.r.t* the tree level increase as one considers higher values of the inert scalar masses, even if the mass-splitting is kept fixed. This is due to the fact that $\lambda_3, \lambda_4, \lambda_5$ grow in magnitude in the process. This feature is easily read from Fig. 5.

We remind that one should also include one-loop corrections to the co-annihilation processes for a more

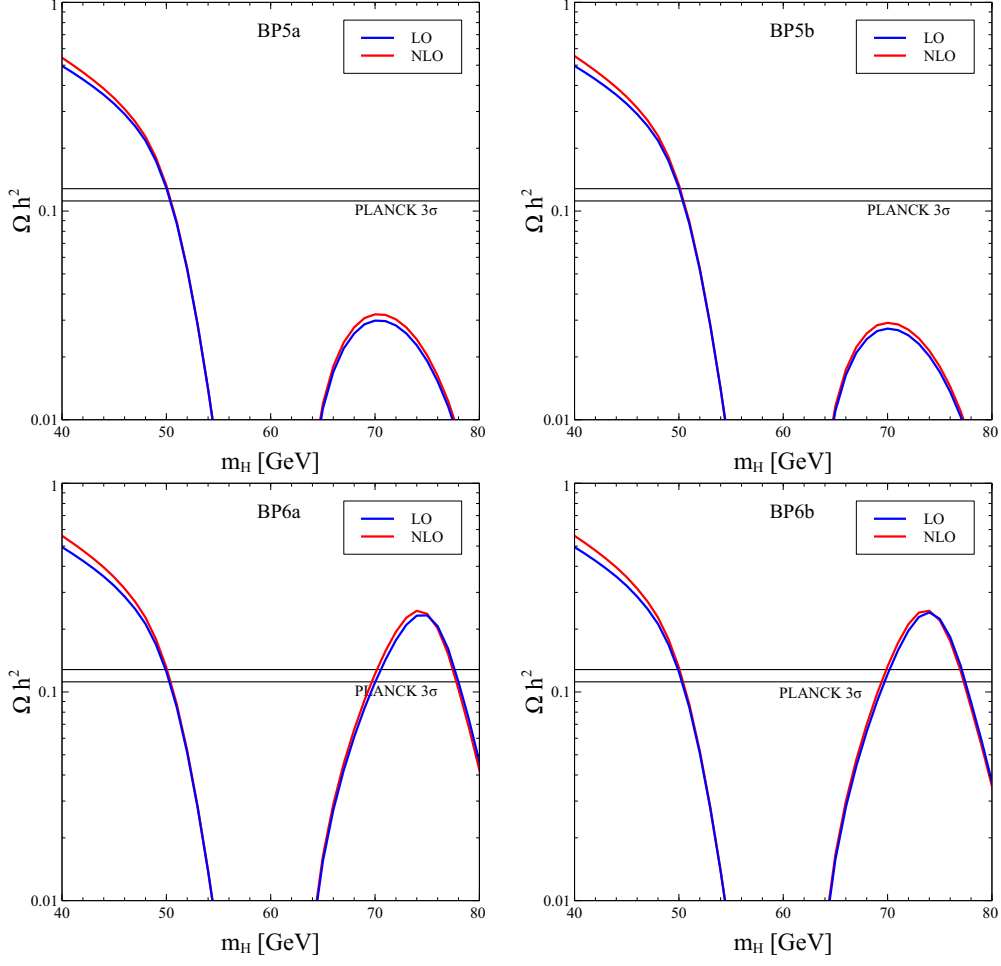


FIG. 3: Variation of the thermal relic with the DM mass. The tree level and one-loop values are denoted by the blue and red curves respectively.

accurate analysis. The crucial co-annihilation mediating HZA , $HW^\mp H^\pm$ and $H^\pm H^\mp Z/\gamma$ vertices shall also receive potentially large corrections from the extended Higgs sector. In addition, a complete NLO analysis of the DM-nucleon scattering rates requires going beyond computing loop corrections to the portal coupling only. To give an example, one loop triangle graphs with A and Z in the internal lines will be encountered. It is also customary to examine the dependence of the results on the renormalisation scheme chosen. A more exhaustive radiative treatment of the present scenario is currently under preparation.

VI. SUMMARY AND OUTLOOK.

In this study we have evaluated one-loop radiative corrections to the dark matter-Higgs interaction in context of the Inert Doublet Model. Canonical constraints from vacuum stability, perturbative unitarity and LHC data have been taken into account. The motivation behind this work is to obtain a measure of

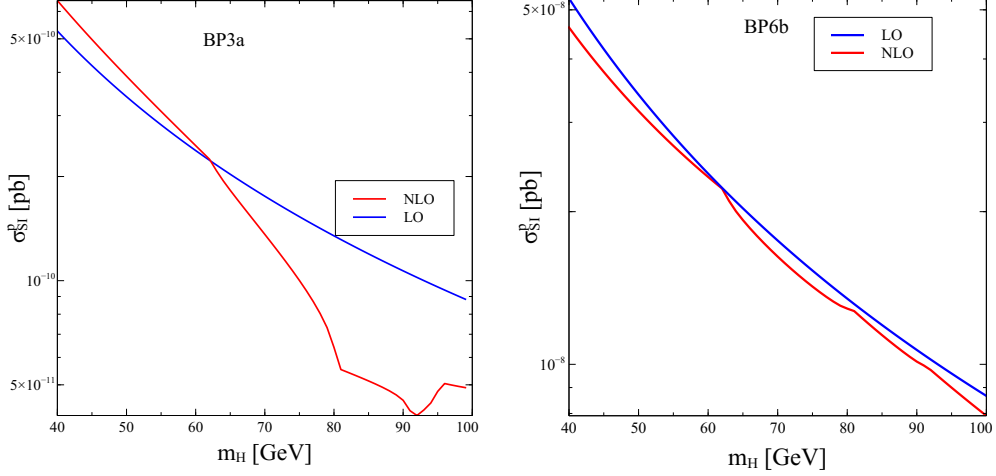


FIG. 4: Variation of the spin-independent cross section with the DM mass. The tree level and one-loop values are denoted by the blue and red curves respectively.

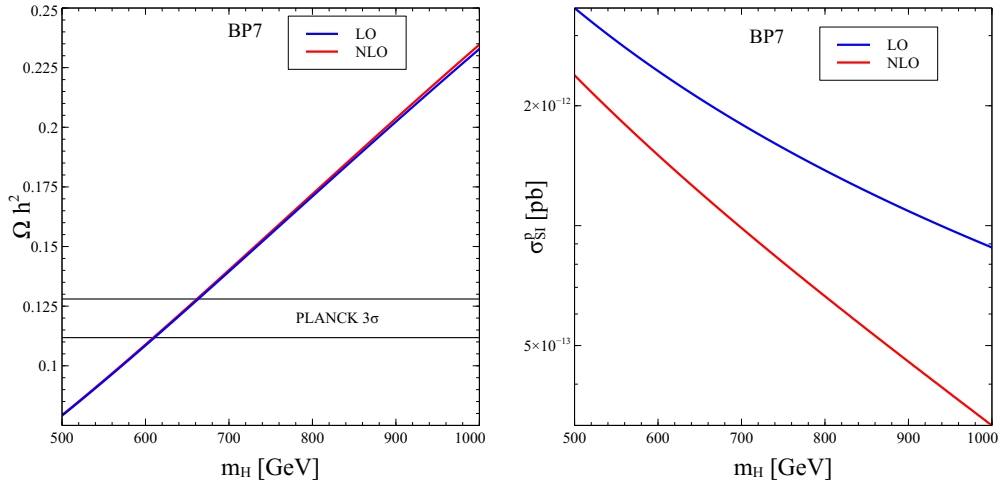


FIG. 5: Variation of the relic density (left) and the spin-independent cross section (right) with the DM mass. The tree level and one-loop values are denoted by the blue and red curves respectively.

deviation from the leading order results, given that an additional doublet furnishes more bosonic degrees of freedom that can participate in a next-to-leading order analysis.

For the dark matter lighter than m_W , the inert doublet cannot be fully decoupled even if the other inert scalars are taken to be heavy. This non-decoupling effect induces sizable loop corrections in the observable quantities. On the other hand, the $m_H > 500$ GeV region witnesses comparatively small radiative shifts in λ_L . This effect can be safely attributed to a by and large decoupled IDM spectrum. However, in the co-annihilation region, a complete picture can only emerge if one incorporates one-loop effects to all the relevant interactions. Moreover, the radiative corrections will also affect the search prospects of a dark matter particle

at the colliders, a promising channel to probe being the monojet + \cancel{E}_T final state. A more exhaustive study on the impact of one-loop corrections to all the relevant interactions in this scenario is presently underway. In all, scalar dark matter models have served as popular frameworks to study interactions of dark matter with the visible world. Through the present study, we have tried to highlight the fact that these models can be made more accurate once they are augmented with relevant radiative corrections.

Acknowledgements

We thank Sun Hao for his help on `LoopTools`. We are grateful to Professor Fawzi Boudjema for his suggestions during the preparation of the manuscript. SB acknowledges the support of the Indo French LIA THEP (Theoretical high Energy Physics) of the CNRS. NC acknowledges the funding available from the Department of Atomic Energy, Government of India, for the Regional Centre for Accelerator based Particle Physics (RECAPP), Harish-Chandra Research Institute.

VII. APPENDIX

We list all the relevant 1PI amplitudes here.

A. Two-point amplitudes.

$$\begin{aligned}
\Pi_{hh}^{1\text{PI}}(p^2) = & \frac{1}{16\pi^2} \left[\frac{3\lambda_1}{2} A_0(m_h^2) + \lambda_1 A_0(m_{G^+}^2) + \frac{\lambda_1}{2} A_0(m_A^2) + \frac{(\lambda_3 + \lambda_4 + \lambda_5)}{2} A_0(m_H^2) + \frac{(\lambda_3 + \lambda_4 - \lambda_5)}{2} A_0(m_A^2) \right. \\
& + \lambda_3 A_0(m_{H^+}^2) + \frac{9\lambda_1^2}{2} v^2 B_0(p^2, m_h^2, m_h^2) + \frac{(\lambda_3 + \lambda_4 + \lambda_5)^2}{2} v^2 B_0(p^2, m_H^2, m_H^2) \\
& + \frac{\lambda_1^2}{2} v^2 B_0(p^2, m_{G^0}^2, m_{G^0}^2) + \lambda_1^2 v^2 B_0(p^2, m_{G^+}^2, m_{G^+}^2) + \frac{(\lambda_3 + \lambda_4 - \lambda_5)^2}{2} v^2 B_0(p^2, m_A^2, m_A^2) \\
& + \lambda_3^2 v^2 B_0(p^2, m_{H^+}^2, m_{H^+}^2) - 2N_c y_t^2 [2A_0(m_t^2) + (4m_t^2 - p^2) B_0(p^2, m_t^2, m_t^2)] + \frac{d}{2} g^2 A_0(m_W^2) \\
& + \frac{d}{4} (g^2 + g'^2) A_0(m_Z^2) + \frac{d}{4} v^2 g^4 B_0(p^2, m_W^2, m_W^2) + \frac{d}{8} v^2 (g^2 + g'^2)^2 B_0(p^2, m_Z^2, m_Z^2) \\
& - \frac{g^2}{2} [2A_0(m_W^2) - A_0(m_{G^+}^2) + (2p^2 + 2m_{G^+}^2 - m_W^2) B_0(p^2, m_W^2, m_{G^+}^2)] \\
& \left. - \frac{g^2 + g'^2}{4} [2A_0(m_Z^2) - A_0(m_{G^0}^2) + (2p^2 + 2m_{G^0}^2 - m_Z^2) B_0(p^2, m_Z^2, m_{G^0}^2)] \right] \quad (16)
\end{aligned}$$

$$\begin{aligned}
\Pi_{HH}^{1\text{PI}}(p^2) = & \frac{1}{16\pi^2} \left[\frac{(\lambda_3 + \lambda_4 + \lambda_5)}{2} A_0(m_h^2) + \lambda_3 A_0(m_{G^+}^2) + \frac{(\lambda_3 + \lambda_4 - \lambda_5)}{2} A_0(m_{G^0}^2) + \frac{3\lambda_2}{2} A_0(m_H^2) + \lambda_2 A_0(m_{H^+}^2) \right. \\
& + \frac{\lambda_2}{2} A_0(m_A^2) + (\lambda_3 + \lambda_4 + \lambda_5)^2 v^2 B_0(p^2, m_h^2, m_H^2) + \lambda_5^2 v^2 B_0(p^2, m_A^2, m_{G^0}^2) \\
& + \frac{(\lambda_4 + \lambda_5)^2}{2} v^2 B_0(p^2, m_{H^+}^2, m_{G^+}^2) + \frac{d}{2} g^2 A_0(m_W^2) + \frac{d}{4} (g^2 + g'^2) A_0(m_Z^2) \\
& - \frac{g^2}{2} [2A_0(m_W^2) - A_0(m_{H^+}^2) + (2p^2 + 2m_{H^+}^2 - m_W^2) B_0(p^2, m_W^2, m_{H^+}^2)] \\
& \left. - \frac{g^2 + g'^2}{4} [2A_0(m_Z^2) - A_0(m_A^2) + (2p^2 + 2m_A^2 - m_Z^2) B_0(p^2, m_Z^2, m_A^2)] \right] \quad (17)
\end{aligned}$$

(18)

$$\begin{aligned}
\Pi_{WW,T}^{1\text{PI}}(p^2) = & \frac{1}{16\pi^2} \left[\frac{g^2}{4} [B_5(p^2; m_H, m_{H^\pm}) + B_5(p^2; m_A, m_{H^\pm})] + g^2 \left(m_W^2 B_0 + \frac{1}{4} B_5 \right) (p^2; m_h, m_W) \right. \\
& + g^2 \left[\left(\frac{1}{4} + 2c_W^2 \right) B_5 + (m_W^2 - 4s_W^2 m_W^2 + m_Z^2 - 8p^2 c_W^2) B_0 \right] (p^2; m_Z, m_W) \\
& \left. + 2s_W^2 [B_5 + (2m_W^2 - 4p^2) B_0] (p^2; m_\gamma, m_W) - \frac{2}{3} g^2 p^2 \right] \quad (19)
\end{aligned}$$

The definition of the $B_5(p^2, m_1^2, m_2^2)$ function can be found in [49].

B. Three-point amplitudes.

$$\begin{aligned}
\Gamma_{HHh}^{1\text{PI}}(p_1^2, p_2^2, q^2) = & \frac{1}{16\pi^2} \left[\frac{3}{2} \lambda_1 (\lambda_3 + \lambda_4 + \lambda_5) v B_0(q^2, m_h^2, m_h^2) + (\lambda_3 + \lambda_4 + \lambda_5)^2 v B_0(p_1^2, m_h^2, m_H^2) \right. \\
& + (\lambda_3 + \lambda_4 + \lambda_5)^2 v B_0(p_2^2, m_h^2, m_H^2) + 3\lambda_1 (\lambda_3 + \lambda_4 + \lambda_5)^2 v^3 C_0(q^2, p_1^2, p_2^2, m_h^2, m_H^2, m_H^2) \\
& + (\lambda_3 + \lambda_4 + \lambda_5)^3 v^3 C_0(q^2, p_1^2, p_2^2, m_h^2, m_H^2, m_H^2) + \frac{3}{2} \lambda_2 (\lambda_3 + \lambda_4 + \lambda_5) v B_0(q^2, m_H^2, m_H^2) \\
& + \lambda_1 \lambda_3 v B_0(q^2, m_{G^+}^2, m_{G^+}^2) + \frac{1}{2} \lambda_1 (\lambda_3 + \lambda_4 - \lambda_5) v B_0(q^2, m_{G^0}^2, m_{G^0}^2) + \lambda_5^2 v B_0(p_1^2, m_{G^0}^2, m_A^2) \\
& + \lambda_5^2 v B_0(p_2^2, m_{G^0}^2, m_A^2) + \frac{1}{2} \lambda_2 (\lambda_3 + \lambda_4 - \lambda_5) v B_0(q^2, m_A^2, m_A^2) \\
& + 4\lambda_1^2 \lambda_5 v^3 C_0(q^2, p_1^2, p_2^2, m_A^2, m_{G^0}^2, m_{G^0}^2) + \lambda_5^2 (\lambda_3 + \lambda_4 - \lambda_5) v^3 C_0(q^2, p_1^2, p_2^2, m_{G^0}^2, m_A^2, m_A^2) \\
& + \lambda_2 \lambda_3 v B_0(q^2, m_{H^+}^2, m_{H^+}^2) + \frac{1}{2} (\lambda_4 + \lambda_5)^2 v B_0(p_1^2, m_{G^+}^2, m_{H^+}^2) + \frac{1}{2} (\lambda_4 + \lambda_5)^2 v B_0(p_2^2, m_{G^+}^2, m_{H^+}^2) \\
& + \lambda_1 (\lambda_4 + \lambda_5)^2 v^3 C_0(q^2, p_1^2, p_2^2, m_{H^+}^2, m_{G^+}^2, m_{G^+}^2) + \lambda_3 (\lambda_4 + \lambda_5)^2 v^3 C_0(q^2, p_1^2, p_2^2, m_{G^+}^2, m_{H^+}^2, m_{H^+}^2) \\
& + \frac{d}{4} g^4 v B_0(q^2, m_W^2, m_W^2) + \frac{d}{8} (g^2 + g'^2)^2 v B_0(q^2, m_Z^2, m_Z^2) \\
& - \frac{(\lambda_3 + \lambda_4 - \lambda_5)}{4} (g^2 + g'^2) \left[p_1^2 C_{21} + p_2^2 C_{22} + 2p_1 \cdot p_2 C_{23} + 4C_{24} + 2p_1 \cdot p_2 C_{11} + 2p_2^2 C_{12} \right. \\
& + (-2p_1 \cdot p_2 - p_1^2) C_0 \left. \right] (p_1^2, p_2^2, q^2, m_A^2, m_Z^2, m_A^2) \\
& - \frac{\lambda_3}{2} g^2 \left[p_1^2 C_{21} + p_2^2 C_{22} + 2p_1 \cdot p_2 C_{23} + 4C_{24} + 2p_1 \cdot p_2 C_{11} + 2p_2^2 C_{12} \right. \\
& + (-2p_1 \cdot p_2 - p_1^2) C_0 \left. \right] (p_1^2, p_2^2, q^2, m_{H^+}^2, m_W^2, m_{H^+}^2) \\
& - \frac{(g^2 + g'^2)^2}{8} v \left[p_1^2 C_{21} + p_2^2 C_{22} + 2p_1 \cdot p_2 C_{23} + 4C_{24} + (3p_1^2 - p_1 \cdot p_2) C_{11} + (3p_1 \cdot p_2 - p_2^2) C_{12} \right. \\
& + (2p_1^2 - 2p_1 \cdot p_2) C_0 \left. \right] (p_1^2, p_2^2, q^2, m_Z^2, m_A^2, m_Z^2) \\
& - \frac{g^4}{4} v \left[p_1^2 C_{21} + p_2^2 C_{22} + 2p_1 \cdot p_2 C_{23} + 4C_{24} + (3p_1^2 - p_1 \cdot p_2) C_{11} + (3p_1 \cdot p_2 - p_2^2) C_{12} \right. \\
& + (2p_1^2 - 2p_1 \cdot p_2) C_0 \left. \right] (p_1^2, p_2^2, q^2, m_W^2, m_{H^+}^2, m_W^2) \Big] \tag{20}
\end{aligned}$$

-
- [1] S. Chatrchyan et al. (CMS), Phys. Lett. **B716**, 30 (2012), 1207.7235.
 - [2] G. Aad et al. (ATLAS), Phys. Lett. **B716**, 1 (2012), 1207.7214.
 - [3] Tech. Rep. ATLAS-CONF-2016-080, CERN, Geneva (2016).
 - [4] Tech. Rep. CMS-PAS-HIG-16-038, CERN, Geneva (2016).
 - [5] P. A. R. Ade et al. (Planck), Astron. Astrophys. **594**, A13 (2016), 1502.01589.
 - [6] N. G. Deshpande and E. Ma, Phys. Rev. **D18**, 2574 (1978).
 - [7] E. Ma, Phys. Rev. **D73**, 077301 (2006), hep-ph/0601225.
 - [8] R. Barbieri, L. J. Hall, and V. S. Rychkov, Phys. Rev. **D74**, 015007 (2006), hep-ph/0603188.
 - [9] L. Lopez Honorez, E. Nezri, J. F. Oliver, and M. H. G. Tytgat, JCAP **0702**, 028 (2007), hep-ph/0612275.

- [10] D. S. Akerib et al. (LUX), Phys. Rev. Lett. **112**, 091303 (2014), 1310.8214.
- [11] R. Agnese et al. (SuperCDMS), Phys. Rev. Lett. **112**, 241302 (2014), 1402.7137.
- [12] M. Ackermann et al. (Fermi-LAT), Phys. Rev. **D82**, 092004 (2010), 1008.3999.
- [13] M. Ackermann et al. (Fermi-LAT), Phys. Rev. Lett. **108**, 011103 (2012), 1109.0521.
- [14] M. Aguilar et al. (AMS), Phys. Rev. Lett. **113**, 121102 (2014).
- [15] M. Aguilar et al. (AMS), Phys. Rev. Lett. **110**, 141102 (2013).
- [16] A. Goudelis, B. Herrmann, and O. Stl, JHEP **09**, 106 (2013), 1303.3010.
- [17] N. Blinov, J. Kozaczuk, D. E. Morrissey, and A. de la Puente, Phys. Rev. **D93**, 035020 (2016), 1510.08069.
- [18] M. A. Daz, B. Koch, and S. Urrutia-Quiroga, Adv. High Energy Phys. **2016**, 8278375 (2016), 1511.04429.
- [19] T. Abe and R. Sato, JHEP **03**, 109 (2015), 1501.04161.
- [20] E. Aprile (XENON1T), Springer Proc. Phys. **148**, 93 (2013), 1206.6288.
- [21] D. S. Akerib et al. (LZ) (2015), 1509.02910.
- [22] M. Gustafsson, E. Lundstrom, L. Bergstrom, and J. Edsjo, Phys. Rev. Lett. **99**, 041301 (2007), astro-ph/0703512.
- [23] P. Agrawal, E. M. Dolle, and C. A. Krenke, Phys. Rev. **D79**, 015015 (2009), 0811.1798.
- [24] S. Andreas, M. H. G. Tytgat, and Q. Swillens, JCAP **0904**, 004 (2009), 0901.1750.
- [25] E. Nezri, M. H. G. Tytgat, and G. Vertongen, JCAP **0904**, 014 (2009), 0901.2556.
- [26] C. Arina, F.-S. Ling, and M. H. G. Tytgat, JCAP **0910**, 018 (2009), 0907.0430.
- [27] J.-O. Gong, H. M. Lee, and S. K. Kang, JHEP **04**, 128 (2012), 1202.0288.
- [28] M. Gustafsson, S. Rydbeck, L. Lopez-Honorez, and E. Lundstrom, Phys. Rev. **D86**, 075019 (2012), 1206.6316.
- [29] E. Lundstrom, M. Gustafsson, and J. Edsjo, Phys. Rev. **D79**, 035013 (2009), 0810.3924.
- [30] Q.-H. Cao, E. Ma, and G. Rajasekaran, Phys. Rev. **D76**, 095011 (2007), 0708.2939.
- [31] E. Dolle, X. Miao, S. Su, and B. Thomas, Phys. Rev. **D81**, 035003 (2010), 0909.3094.
- [32] X. Miao, S. Su, and B. Thomas, Phys. Rev. **D82**, 035009 (2010), 1005.0090.
- [33] L. Wang and X.-F. Han, JHEP **05**, 088 (2012), 1203.4477.
- [34] P. Osland, A. Pukhov, G. M. Pruna, and M. Purmohammadi, JHEP **04**, 040 (2013), 1302.3713.
- [35] A. Belyaev, G. Cacciapaglia, I. P. Ivanov, F. Rojas, and M. Thomas (2016), 1612.00511.
- [36] A. Arhrib, Y.-L. S. Tsai, Q. Yuan, and T.-C. Yuan, JCAP **1406**, 030 (2014), 1310.0358.
- [37] A. J. Ilnicka, M. Krawczyk, and T. Robens, PoS **EPS-HEP2015**, 143 (2015), 1510.04159.
- [38] P. Poulose, S. Sahoo, and K. Sridhar (2016), 1604.03045.
- [39] A. Arhrib, R. Benbrik, J. El Falaki, and A. Jueid, JHEP **12**, 007 (2015), 1507.03630.
- [40] S. Kanemura, M. Kikuchi, and K. Sakurai (2016), 1605.08520.
- [41] M. Klasen, C. E. Yaguna, and J. D. Ruiz-Alvarez, Phys. Rev. **D87**, 075025 (2013), 1302.1657.
- [42] B. W. Lee, C. Quigg, and H. B. Thacker, Phys. Rev. **D16**, 1519 (1977).

- [43] A. G. Akeroyd, A. Arhrib, and E.-M. Naimi, Phys. Lett. **B490**, 119 (2000), hep-ph/0006035.
- [44] J. Horejsi and M. Kladiva, Eur. Phys. J. **C46**, 81 (2006), hep-ph/0510154.
- [45] B. Gorczyca and M. Krawczyk (2011), 1112.5086.
- [46] M. Baak, J. Cth, J. Haller, A. Hoecker, R. Kogler, K. Mnig, M. Schott, and J. Stelzer (Gfitter Group), Eur. Phys. J. **C74**, 3046 (2014), 1407.3792.
- [47] G. Aad et al. (ATLAS, CMS), JHEP **08**, 045 (2016), 1606.02266.
- [48] S. Kanemura, Y. Okada, E. Senaha, and C.-P. Yuan, Phys. Rev. D **70**, 115002 (2004).
- [49] K. Hagiwara, S. Matsumoto, D. Haidt, and C. S. Kim, Z. Phys. **C64**, 559 (1994), [Erratum: Z. Phys.C68,352(1995)], hep-ph/9409380.